Fig. 3b. Each term in Fig. 3a and 3b distributes quite similarly. For both short bubbles, the production term attains its maximum and begins to decrease well before the reattachment.

Spatial Distributions

In Fig. 4, the points where the production by shear stress $[-\overline{uv}(\partial\bar{U}/\partial y + \partial\bar{V}/\partial x)]$ reaches its maximum (point A in Fig. 4) and where the transverse diffusion term $(-\partial\overline{vk}/\partial y)$ changes its sign, that is, zero diffusion points, points B and C, are shown. The position where the gradient of the mean longitudinal velocity, $\partial\bar{U}/\partial y$, reaches its maximum (point D) and the maximum slope thickness δ_ω are also plotted in Fig. 4 to indicate the shear layer growth. The same method discussed regarding spatial distributions in Fig. 4 was used in Ref. 5. The maximum slope thickness, which is a measure of the shear layer growth, is defined by $\delta_\omega \equiv \overline{U_e}/(\partial\bar{U}/\partial y)_{\max}$, where $\overline{U_e}$ denotes the maximum $\bar{U}$ for each chordwise station. Distributions of δ_ω are indicated by $\updownarrow$ in Fig. 4. The vertical scale is enlarged for clarity.

The chordwise distributions of the maximum production points A and maximum velocity gradient points D almost coincide. The distance between the zero diffusion points (B and C) increases toward the reattachment. As this distance increases, the thickness of the shear layer also grows toward the reattachment, which indicates the effects of turbulent diffusion. However, this growth is located outside of the reverse flow region.

Conclusions

In summary, results of the short bubble formed on the NACA 0012 indicate that the production term has the largest contribution to the growth of turbulent energy that coincides with those of the short bubble formed on NACA 63-009. The present results also indicate that the width of the separated shear layer increases toward the reattachment due to the effects of transverse diffusion. The results for this Note were measured more accurately than those previously measured for a NACA 63-009 using and can be used as basic information and data for turbulent developments inside a short bubble.

References

[1]Tani, I., "Low-Speed Flows Involving Bubble Separation," *Progress in Aeronautical Sciences*, Vol. 5, Pergamon, New York, 1964, pp. 70–103.

[2]Fitzgerald, E. J., and Mueller, T. J., "Measurements in a Separation Bubble on an Airfoil Using Laser Velocimetry," *AIAA Journal*, Vol. 28, No. 4, 1990, pp. 584–592.

[3]Rinoie, K., Shingo, M., and Sato, J., "Measurements of Short Bubble and Long Bubble Formed on NACA 63-009 Airfoil," *Journal of the Japan Society for Aeronautical and Space Sciences*, Vol. 38, No. 436, 1990, pp. 251–257 (in Japanese).

[4]Driver, D. M., and Seegmiller, H. L., "Features of a Reattaching Turbulent Shear Layer in Divergent Channel Flow," *AIAA Journal*, Vol. 23, No. 2, 1985, pp. 163–171.

[5]Rinoie, K., Shirai, Y., and Sunada, Y., "Behavior of Separated and Reattaching Flow Formed over a Backward Facing Step," *Transactions of the Japan Society for Aeronautical and Space Sciences*, Vol. 45, No. 147, 2002, pp. 20–27.

[6]Hata, K., Rinoie, K., Takemura, N., and Sunada, Y., "Experimental Studies of Low Frequency Velocity Disturbances Observed in Short Bubble Formed on Airfoil," *Journal of Japan Society for Aeronautical and Space Sciences*, Vol. 50, No. 582, 2002, pp. 293–300 (in Japanese).

[7]Brunn, H. H., *Hot-Wire Anemometry*, Oxford Univ. Press, Oxford, 1995, pp. 405–445.

[8]Petrie, H. L., Samimy, M., and Addy, A. L., "Laser Doppler Velocity Bias in Separated Turbulent Flows," *Experiments in Fluids*, Vol. 6, No. 2, 1988, pp. 80–88.

W. Devenport
Associate Editor

Experimental Study of a Weak Vortex–Normal Shock Interaction

I. M. Kalkhoran* and C. Paek†
Polytechnic University, Brooklyn, New York 11201

Introduction

INTERACTION of a streamwise vortex with an otherwise normal shock front, commonly called normal shock wave–vortex interaction, constitutes a problem of some importance in supersonic flows. Interactions of this type are commonplace on supersonic aircraft and missiles, where vortices generated by forward components can encounter shock waves in close proximity to wings and control surfaces present in their passages. These interactions are in general undesirable from a performance standpoint because they may lead to loss of lift, increase in drag, and may alter the stability and control characteristics of the vehicle. Another deleterious possibility is the ingestion of streamwise vortices by the air intake system of a supersonic vehicle resulting in decreased engine performance, blockages of the engine intake, or possibly inlet unstart.

Numerous experimental studies of the interaction between isolated streamwise vortices and otherwise normal shock waves have been carried out.[1–5] In summary, the results of these studies have revealed vortex breakdowns for vortex–shock wave combinations exceeding certain strengths. Moreover, both experimental and theoretical studies have indicated an inverse relationship between the vortex strength and the shock wave intensity at breakdown.[6] It is also clear that the interaction structure depends strongly on the methodology used to generate streamwise vortices and, hence, on the distribution of flow properties within vortex cores. In their work, Delery et al.[2] obtained a shock-induced vortex breakdown limit relating a vortex intensity parameter defined by $\tau_{\max} = (V_\theta)_{\max}/V_\infty$ to the strength of the normal shock wave as determined by the freestream Mach number. In a subsequent study, Kalkhoran et al.[5] carried out an experimental study of the interaction of streamwise wing-tip vortices with otherwise planar normal shock fronts at Mach 2.49. These experiments revealed conical vortex distortion patterns possessing many of the visual characteristics of incompressible vortex breakdown. In a later study,[7] these vortex distortions were shown to be distinct forms of vortex breakdown possessing many of the characteristics of the well-documented low-speed vortex breakdown with a region of reversed flow and stagnation points on the vortex axis.

Considering the simplified situation of the interaction between an axisymmetric streamwise vortex and a planar normal shock wave, the axial Mach number of the vortex is significantly reduced from supersonic to subsonic values when crossing the shock. On the other hand, the swirl component of the Mach number, being approximately tangent to the shock surface, is only marginally influenced. Consequently, the swirl ratio of the vortex will significantly increase in crossing the shock front with the jump in the swirl ratio being directly proportional to the strength of the shock, which in turn is determined by the freestream Mach number. This change in the swirl ratio of the vortex must have a significant effect on the stability of the vortex and consequently on the structure of the downstream flow. Generally, vortex breakdown occurs when the swirl ratio reaches a critical value beyond which a coherent vortical

Received 16 May 2003; revision received 8 January 2004; accepted for publication 27 February 2004.

*Associate Professor, Department of Mechanical, Aerospace, and Manufacturing Engineering. Senior Member AIAA.

†Graduate Student, Department of Mechanical, Aerospace, and Manufacturing Engineering.

structure cannot physically exist. In light of this behavior, an interesting aspect of the normal shock wave–vortex interaction problem is whether a coherent vortex could withstand the severe jump in its axial Mach number from supersonic to subsonic values without a major reorganization of its structure. Alternatively, interactions not leading to vortex breakdown would indicate existence of a well-defined vortical structure on either side of the shock that have nearly identical tangential Mach numbers but distinct axial Mach numbers, namely, supersonic upstream of the shock and subsonic downstream. Because Ref. 5 only considered the interaction of moderate ($\tau_{max} = 0.18$) and strong ($\tau_{max} = 0.32$) vortices, the behavior of a weak vortex during normal shock wave–vortex interaction is of interest. The present experimental effort was undertaken to investigate the interaction between a weak streamwise vortex and an otherwise planar normal shock front in an attempt to expand upon the results of the previous study reported in Ref. 5.

Experimental Arrangement

The current study was carried out in a 38.1×38.1 cm supersonic blowdown wind tunnel at a nominal test-section Mach number of 2.49. The stagnation pressure and temperature for these experiments were 0.45 MPa and 290 K, respectively, resulting in a unit Reynolds number of 4.3×10^7 per meter. A generic illustration of the experimental arrangement is shown in Fig. 1. The interaction experiments utilized a vortex generator consisting of a rectangular half-wing with a diamond-shaped airfoil section of 8 deg half-angle, a chord length of 50.8 mm, and a span of 165.1 mm. The normal shock generator had a square 63.5×63.5 mm inlet and was 156 mm long placed 152.4 mm downstream of the wing. In these experiments, a planar normal shock was created in front of the inlet by choking the flow through the inlet using an adjustable obstruction at its exit. In the absence of the vortex generator, this arrangement resulted in the formation of a planar normal shock with a minimum amount of flow spillage.[5]

Experimental Results and Discussion

In an attempt to quantify characteristics of the weak vortex, flowfield properties in the core region were measured by means of five-hole and four-hole conical probes. The scheme utilized a 30-deg, four-hole conical probe to supply cone surface pressures and a 30-deg, five-hole conical probe for the measurements of pitot pressure. Calibration curves for the conical probe were constructed using the method of Ref. 8 by means of a conical Euler solver as opposed to a conventional experimental calibration of the probe. These measurements were performed a distance of 113 mm downstream of the vortex generator trailing edge. Details of the measurement technique may be found in Ref. 8.

Figures 2 and 3 illustrate distribution of the flow properties in the vortex as obtained from vertical (spanwise with respect to the half-wing in Fig. 1) surveys through the vortex core. Conventional

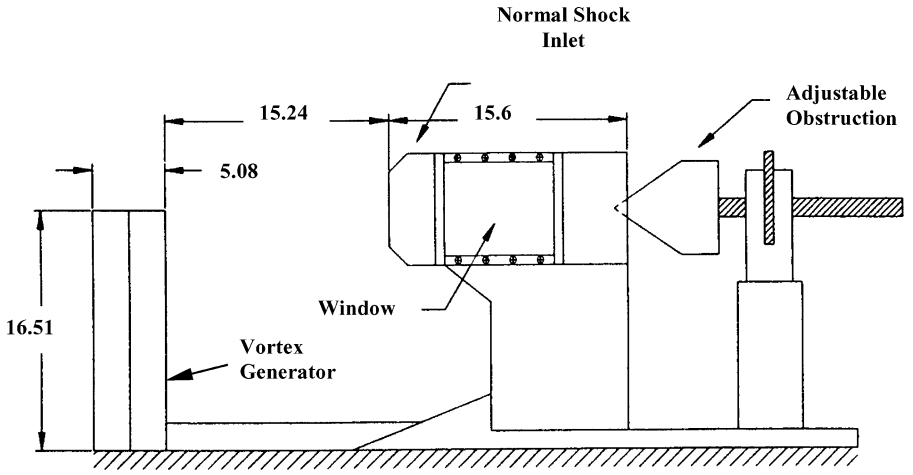

Fig. 1 Experimental arrangement for interaction of a weak vortex with a normal shock. All dimensions are in centimeters.

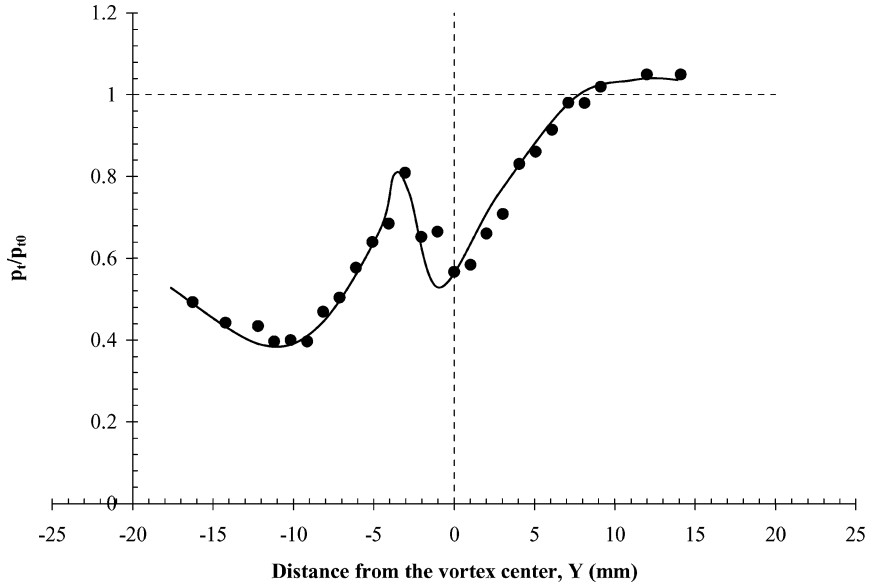

Fig. 2 Total pressure distribution in the core of the weak vortex.

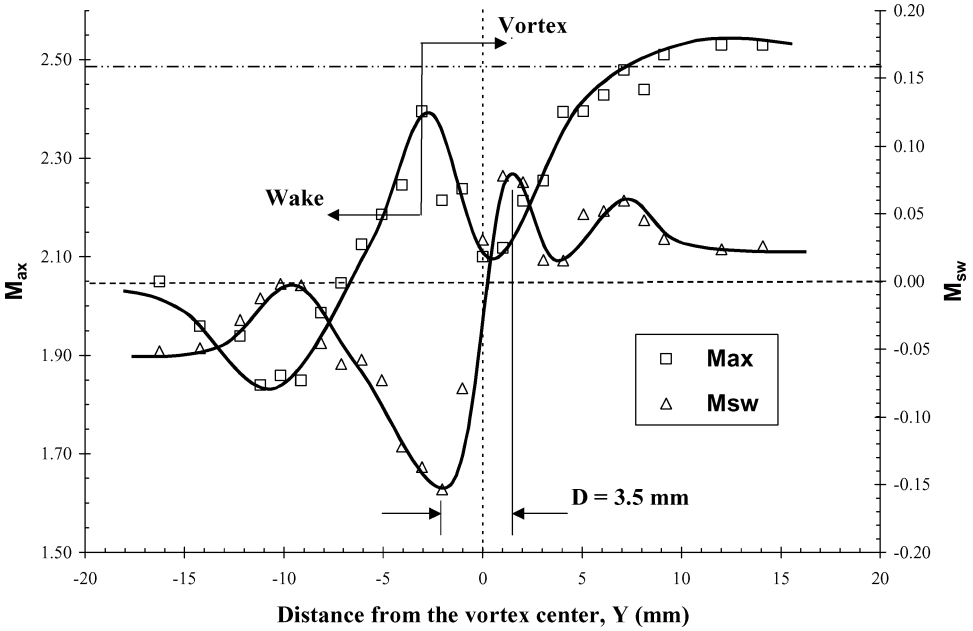

Fig. 3 Axial and tangential Mach-number distributions in the core of the weak vortex.

uncertainty analysis of the measured quantities indicates that the maximum uncertainty values in the measured total pressure, axial, and swirl Mach numbers are 0.064, 0.04, and 0.001, respectively. As indicated in Fig. 2, similar to the moderate and strong vortices of Ref. 5, the weak vortex is a region of total pressure deficit with the minimum total pressure $P_t/P_{t0} = 0.55$ at the vortex axis. Outboard of the vortex, the total pressure is seen to return to a value close to that of the freestream a distance of 9 mm above the vortex center. Inboard of the vortex, the total pressure is seen to rapidly rise to a value of $p_t/p_{t0} = 0.8$ approximately 4 mm below the vortex axis before it is significantly influenced by the vortex generator wake.

Distribution of the axial and tangential Mach numbers in the core of the vortex is shown in Fig. 3. This figure indicates that the weak vortex contains a wakelike axial Mach-number profile with a minimum value of 2.08 at the vortex center. An examination of the axial Mach-number distribution indicates a rapid return toward the freestream value outboard of the wing while, inboard of the wing, the axial Mach number increases to about 2.4 approximately 4 mm below the vortex center before being significantly influenced by the vortex generator wake at distances farther inboard. Of particular importance to the present interaction studies is the significant axial Mach-number deficit in the wake region of the half-wing. As evident from Fig. 3, unlike the moderate and strong vortices of Ref. 5, the weak vortex has a minimum axial Mach number of 1.82 in the wake approximately 10 mm below the vortex axis. At distances below $Y = -10$ mm, the wake region shows a rather unusually nonsymmetric behavior where the axial Mach number continuously increases to $M_{ax} = 2.05$ at the last measurement location of $Y = -16$ mm. Although the exact cause of this behavior of the wake region is not known at the present time, the close proximity of the weak vortex and the wake is likely due to the smaller downwash of the weak vortex in comparison to the moderate and strong vortices of Ref. 5. In summary, the axial Mach-number profile illustrates a trend to be expected of a streamwise vortex, with the exception of the strong wake effect at distances below $Y = -4$ mm.

An examination of the tangential Mach-number distribution indicates a tightly wound vortex with a "Burgers-like" swirl Mach-number profile with an inner solid-body rotation surrounded by an outer region with swirl similar to an irrotational vortex. The maximum swirl Mach number of the vortex is seen to be $M_\theta = 0.08$ outboard and $M_\theta = 0.15$ inboard of the vortex axis. The nonsymmetric behavior of the tangential Mach-number profile was also observed in the core of moderate and strong vortices of Ref. 5 and is again attributed to the wake of the half-wing. Based on these values, the characteristic maximum swirl ratio of the vortex is found to be $\tau_{max} = 0.07$. As expected, this value is significantly lower than that of the moderate ($\tau_{max} = 0.18$) and strong ($\tau_{max} = 0.32$) vortices. Consequently, interaction of this vortex with a normal shock was expected to represent an interaction with significantly reduced intensity. As illustrated in Fig. 3, the vortex has a viscous core diameter of approximately 3.5 mm (as defined by the peak-to-peak swirl Mach number). Note that outboard of the vortex core the swirl profile indicates a gradual leveling of the swirl Mach number, whereas inboard of the wing, the swirl profile is again influenced by the vortex generator wing at distances below $Y = -10$ mm. The pertinent flow properties characterizing the weak vortex are summarized in Table 1. These properties constitute the upstream boundary conditions for the interaction problem, which in turn dictate the downstream flowfield properties and ultimately determine the mutual influence of the shock and the vortex on one another.

Table 1 Flow properties in the core of the weak vortex

Property	Value
Centerline static pressure $p/p_{t\infty}$	0.062
Centerline total pressure $p_t/p_{t\infty}$	0.567
Centerline axial Mach no. M_{ax}	2.08
Maximum swirl ratio τ_{max}	0.07

Having established the flow properties in the vortex core, interaction experiments were initiated by placing the pitot-type inlet downstream of the vortex generator half-wing. Figure 4 is a spark shadowgraph of the flowfield generated during the encounter. In Fig. 4 the dashed lines indicate the approximate trace of the vortex as determined from the conical probe measurements because the vortex trajectory is not as clear in the shadowgraph as those of the moderate and strong vortices of Ref. 5 due to a smaller density gradient in the core region. An examination of Fig. 4 clearly illustrates an upstream bulging of the shock front as a result of the interaction. The bulging of the shock in response to the presence of the vortex is seen to start slightly above the outer edge of the vortex and continues a sensible distance below the vortex core. The upstream displacement of the shock is caused by the wakelike axial Mach number in the vortex in a manner consistent with the reduced Mach number ahead of a planar normal shock front. Outboard of the vortex, the bulged-forward shock merges with the undisturbed shock wave near the top of the inlet, with the shock being normal to the freestream direction.

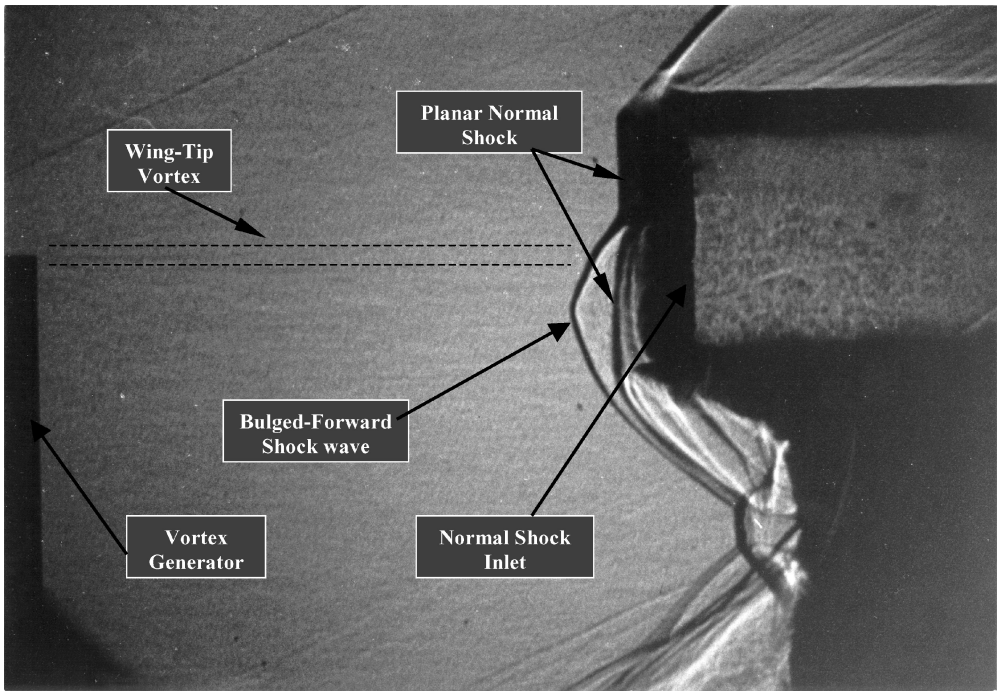

Fig. 4 Spark shadowgraph of the flowfield during interaction of the weak vortex with an otherwise normal shock wave.

The leading portion of the bulged-forward shock front is seen to be situated approximately 13 mm upstream of the undisturbed shock wave. As stated earlier, the vortex generator wake has a minimum axial Mach number of 1.82 a distance 10 mm below the vortex center. This corresponds closely with the approximate location of the most upstream position of the bulged-forward shock front. Interestingly, an examination of the swirl component of the Mach number clearly indicates a negligible swirl at this location, making the reduced axial Mach number in the wake entirely responsible for this local bulging of the shock front. At distances below $Y = -10$ mm, the shock wave is seen to curve downstream before merging with the shock wave associated with the inlet support structure. Again, as indicated in the Mach-number distribution plot of Fig. 3, this is in response to the gradual increase of the axial Mach number in this region. Evidence of the planar normal shock front is also present in the shadowgraph of Fig. 4 just downstream of the bulged-forward shock structure. The presence of this planar normal shock wave indicates that the distortion of the shock is a local phenomenon associated with the reduced Mach numbers in the vortex and the wake regions. Conversely, outside of these regions where the inlet encounters uniform flow, the shock remains normal and planar in a manner consistent with the case where the vortex is not present.

An interesting aspect of the generated flowfield is the lack of presence of a conical vortex distortion pattern, which was shown in Refs. 5 and 6 to be the major defining characteristic associated with a supersonic vortex breakdown involving a vortex with wakelike axial Mach-number profile. For the weak vortex examined in the present study ($\tau_{\max} = 0.07$), the results of Refs. 2 and 6 indicate that a vortex breakdown is not expected to occur. Furthermore, as discussed earlier, the most serious effect of the interaction appears to be due to the interaction of the vortex generator wake with the shock wave. In summary, based on a comparison of Fig. 4 with those obtained during moderate and strong interactions of Ref. 5 leading to vortex breakdown, it is clear that the flowfield reorganization characteristic of vortex breakdown is not induced by the weak vortex. This is despite the fact that, for the present configuration, the maximum swirl ratio of the vortex nearly doubles in crossing the shock front. It is also interesting to note the highly turbulent flow inside the inlet as a result of amplification of turbulent fluctuations when the viscous wake is processed by the nearly strong normal shock front.

Conclusions

In an attempt to expand upon the results of previous normal shock wave–vortex interaction studies, an experimental investigation of the interaction between a weak vortex and an otherwise normal shock wave was carried out in a Mach 2.49 flow. Measurements of the flow properties in the core region of the weak vortex indicated reduced total pressures, a wakelike axial Mach-number distribution, and a Burgers-like swirl profile. These parameters contained identical trends to those measured for moderate and strong vortices but with much lower intensities. These measurements further revealed a significant reduction of the axial Mach number in the vortex generator wake where the measured axial Mach number was seen to be lower than that at the vortex axis. Interaction of the weak vortex with a normal shock front revealed a local bulging of the shock wave in the upstream direction. The upstream bulging of the shock wave was seen to be more pronounced in the wake region where the Mach number was a minimum. Examination of the generated flowfield did not reveal a vortex distortion pattern comparable to the supersonic vortex breakdown observed during previous shock wave–vortex interaction studies.

References

[1]Zatoloka, V., Ivanyushkin, A. K., and Nikolayev, A. V., "Interference of Vortexes with Shocks in Airscoops. Dissipation of Vortexes," *Fluid Mechanics, Soviet Research*, Vol. 7, No. 4, 1978, pp. 153–158.

[2]Delery, J., Horowitz, E., Leuchter, O., and Solignac, J. L., "Fundamental Studies on Vortex Flows," *La Recherche Aerospatiale* (English ed.), No. 2, 1984, pp. 1–24.

[3]Metwally, O., Settles, G., and Horstman, C., "An Experimental Study of Shock Wave/Vortex Interaction," AIAA Paper 89-0082, Jan. 1989.

[4]Cattafesta, L. N., and Settles, G. S., "Experiments on Shock/Vortex Interaction," AIAA Paper 92-0315, Jan. 1992.

[5]Kalkhoran, I. M., Smart, M. K., and Betti, A., "Interaction of Supersonic Wing-Tip Vortices with a Normal Shock," *AIAA Journal*, Vol. 34, No. 9, 1996, pp. 1855–1861.

[6]Kalkhoran, I. M., and Smart, M. K., "Aspects of Shock Wave-Induced Vortex Breakdown," *Progress in Aerospace Sciences*, Vol. 36, 2000, pp. 63–95.

[7]Kalkhoran, I. M., Smart, M. K, and Wang, F. Y., "Supersonic Vortex Breakdown During Vortex/Cylinder Interaction," *Journal of Fluid Mechanics*, Vol. 369, 1998, pp. 351–380.

[8]Smart, M. K., Kalkhoran, I. M., and Bentson, J., "Measurements of Supersonic Wing Tip Vortices," *AIAA Journal*, Vol. 33, No. 10, 1995, pp. 1761–1768.

M. Sichel
Associate Editor

Vortex Shedding and Spacing of a Rotationally Oscillating Cylinder

T. Lee,* D. Birch,† and P. Gerontakos†
McGill University, Montreal, Quebec H3A 2K6, Canada

Introduction

THE possibility of the suppression or elimination of vortex shedding is of considerable practical interest from the standpoint of wake modification and reduction of drag, as well as of flow-induced vibration. Various passive and active control schemes have been attempted to affect the vortex wake formation process. Recently, it has been shown that a considerable amount of control of the cylinder vortex wake can be achieved through rotational oscillation and that when the flow takes place in a fluid relative to a rotationally oscillating cylinder, a new series of flow phenomena could arise.[1–4]

Tenada[1] studied the effects of rotational oscillation for $Re(=du_\infty/\nu$, where ν is the fluid viscosity) ranging between 30 and 300, and indicated that, at very high oscillation frequency f_0 and amplitude, the dead-fluid region behind a cylinder and the vortex-shedding process could be nearly eliminated. The amplitude is given by $\Omega_1 = \pi\Delta\theta f_0 d/2u_\infty > 7$–$27$, where $\Delta\theta$ is the peak-to-peak amplitude in degrees, d is the cylinder diameter, and u_∞ is the freestream velocity. Recently, Filler et al.[2] studied experimentally the frequency response of the shear layers separating from a circular cylinder subjected to small-amplitude oscillations, that is, $\Omega_1 \leq 0.03$, for $Re = 250$–1200, and observed a coupling of the cylinder oscillations with both modes of vortex shedding, that is, shear-layer vortices and primary Kármán vortex shedding. Filler et al. also reported that by rotationally oscillating the cylinder at or near the natural Kármán frequency, the shear-layer instability was promoted and the Kármán mode of vortex shedding was also affected. On the other hand, Tokumaru and Dimotakis[3] have shown that large-amplitude ($\Omega_1 \leq 16$) and high-frequency ($f_0/f_k = 1$–20, where f_k is the natural Karman shedding frequency) rotational oscillations, together with the spinning of the cylinder, can suppress the vortex shedding and produce significant reduction in the profile drag acting on the cylinder at $Re = 1.5 \times 10^4$.

The objective of this study was to investigate the variation of the lateral and longitudinal spacings of the shed vortices and the vortex formation with the cylinder oscillation at $Re = 1.75 \times 10^3$ by the use of hydrogen-bubble and particle streakline flow visualization methods. Special attention was given to the study of the type of wake synchronization that might occur throughout an intermediate oscillation range ($f_0/f_k < 4$ and $\Omega_1 \leq 1.0$), between those of Filler et al. and Tokumaru and Dimotakis.

Received 24 December 2002; revision received 27 October 2003; accepted for publication 14 January 2004.

*Associate Professor, Department of Mechanical Engineering. Member AIAA.

†Graduate Research Assistant, Department of Mechanical Engineering.

Experimental Methods

The experiment was conducted in a $45 \times 45 \times 180$ cm water towing tank. A polished hollow aluminum circular cylinder with a diameter of 2.54 cm and a length of 40 cm, fitted with an endplate, mounted vertically in the center of the tow carriage, was used as the test model. The origin of the coordinates was taken at the center of the cylinder with the x and y axes measured in the streamwise and transverse directions, respectively. The cylinder was rotated sinusoidally with $\Omega(t) = \Omega_1 \sin 2\pi f_0 t$ by a stepper motor. The cylinder rotary motion was monitored with a TRW type DP801 potentiometer (with an accuracy of ± 0.1 deg). A dc servomotor with a towing speed varying from 4 to 12 cm/s was used to drive the towing carriage. The initial acceleration and final deceleration of the towing speeds were carefully programmed to minimize the flow disturbance or nonuniformity induced by the impulsive motion of the cylinder and their effects on the vortex formation. The frequency of the vortex wake and the uniformity of the flow were also measured directly by the use of a cylindrical hot-film probe (TSI Model 1210-20W) incorporating an HP 3584A full Fourier transform (FFT) spectrum analyzer and an oscilloscope, respectively. Long-exposure particle streaklines and hydrogen-bubble flow visualizations were also recorded on Kodak T-MAX 400 film with a 35-mm Nikon camera and a 30-Hz video camera, respectively. The video film was studied frame-by-frame to determine the changes in the pattern and spacing of the shed vortices.

Results and Discussion

Figs. 1b–1i show the vortex streets for $f_0 < 4f_k$ at $\Omega_1 = 1.0$ with $Re = 1.75 \times 10^3$. Depending on the values of oscillation frequency and amplitude, three fundamental types of vortex lock-on were observed. At $f_0 = \frac{1}{2} f_k$, a subharmonic form of lock-on took place whereby the vortex shedding approached a single line of vortices of alternate signs with a significantly increased longitudinal, l, spacing and a vanishing lateral, h, spacing of the vortex street, that is, near the limit of vortex spacing ratio $h/l = 0$, Fig. 1b, compared to that of a stationary cylinder (Fig. 1a). In contrast, at oscillation frequencies near or at the Kármán frequency ($f_0 = 0.75$–$1.25 f_k$), the lock-on took place as vortices were shed alternately from the cylinder to form an altered vortex street (Figs. 1c–1e), similar to the classical Kármán vortex street but with different values of h and l. The lock-on phenomena were found to be similar to the results of Griffin and Ramberg[5] for a cylinder vibrating laterally with the vortex and vibration frequency synchronized. Figures 1f–1i show that for a cylinder oscillated at a multiple of the Kármán frequency ($f_0 = 1.5$–$4 f_k$), the vortex street took on an appearance of largely parallel vortex shedding mode, specifically, a contracted alternating vortex pattern like a normal vortex street but with vortex centers parallel to the wake centerline, resembling jetlike flows. No discernible vortex formation region and shear-layer instability were observed in the present experiment, as opposed to the observed coupling of the small-amplitude cylinder oscillation with both secondary and primary vortices of Filler et al. For the present range of oscillation conditions investigated, the separated shear layers were highly disturbed and with sufficient vorticity, thus allowing a growing vortex behind the oscillating cylinder to roll up quickly, eliminating or suppressing the necessity of drawing the opposite shear layer across the wake (as opposed to the natural vortex formation process existing behind a stationary cylinder, as proposed by Gerrard[6]). Also, an oscillation amplitude as low as $\Omega_1 = 0.25$, instead of a minimum value of Ω_1 of 2 as recommended by Tokumaru and Dimotakis,[3] was needed to send the vorticity stored in the boundary layer into the wake in a regular manner.

Figures 1j–1n also show that, depending on the values of f_0 and Ω_1, the wake unlocked from the oscillation of the cylinder and rendered dramatic change in the vortex shedding modes. The conceptual diagrams of the periodic and synchronized vortex patterns are shown in Fig. 2. Similar to the work of Williamson and Roshko,[7] who studied the synchronized wake behind a cylinder subjected to a sinusoidal trajectory in an X–Y towing tank, the lock-on vortex streets shown in Figs. 1c–1i can be represented by the $2S$ vortex mode, which indicates that in each one-half cycle a vortex was